INVESTIGATION OF IMPROVEMENT CAPABILITIES OF MULTIDIMENSIONAL POLYHARMONIC EXTRAPOLATION ALGORITHM

V.V. Badanov, A.P. Evseev

Nizhny Novgorod State University

Different methods of extrapolation are often used in modern data processing and automatic control systems. Nowadays, spectral characteristics calculated by the Fast Fourier Transform are widely used while processing signals of different kinds. In particular, the solution of an extrapolation problem (which is based on the postulate of preservation of patterns working in the forecast interval and in the past history interval) is easily formulated and implemented in terms of spectral characteristics.

One of the promising algorithms which follow this approach rather effectively and fast is a polyharmonic extrapolation algorithm (PEA) based on computing a model of source time-series in the form of spectral characteristics of some four-terminal circuit.

The algorithm described in previous publications [1] is basic and allows a number of modifications and generalization to multidimensional cases due to the transparency of physical interpretation. Multidimensional extrapolation algorithms can be used, for instance, to increase the accuracy of a set of one-dimensional forecasts, because one-dimensional time-series from different sources can be correlated to each other. Therefore, it is possible to extrapolate a set of such time-series simultaneously, not separately. Such a complex forecast makes it possible to achieve better forecast accuracy due to the employment of variation of spectral characteristics patterns not only in time dimension, but also in other dimensions.

Unlike the one-dimensional PEA, detailed investigations of a multidimensional PEA have not been performed up to now. In this paper we attempted to identify and interpret some disadvantages of a multidimensional polyharmonic extrapolation algorithm. We also proposed methods of extrapolation accuracy improvements and examined them by computer simulations on model time-series.

In particular, some inaccuracies of the multidimensional algorithm are observed during the extrapolation of a two-dimensional time-series which represents a spectrogram of a sine signal with frequency modulation (e.g. linear time dependency of carrier frequency). In this case besides the useful (extrapolated) time-series, some undesirable "echo" appears in the forecast interval under certain conditions and distorts the useful time-series. The problem of detection and suppression of such undesirable "echo" can be partly solved by increasing the order of Fourier-transform used in the algorithm. Fourier-transform with adding zeros to the size which is equal to the nearest number of the power of 2 was used in the simplest version of the polyharmonic extrapolation algorithm. However, a greater (several orders) increase of the size of Fourier-transform makes it possible to trace the structure of spectrum details more carefully due to calculating spectral characteristics with a less frequency step. Therefore, the possibility to find a peak of a harmonic

curve is increased with the Fourier-transform size growth. The approach under discussion suppresses the amplitude of the undesirable "echo" in the forecast interval.

In this investigation of the multidimensional polyharmonic extrapolation algorithm which was performed by computer simulation with different kinds of test time-series, we have found certain types of time-series on which the multidimensional PEA shows insufficient accuracy. We also proposed several methods which enable us to increase the accuracy of extrapolation to some extent.

[1] Баданов В.В., Евсеев А.П., Евсеев Д.А. //Вестник Нижегородского университета им. Н.И.Лобачевского. Серия Радиофизика. Н.Новгород: Изд-во ННГУ, 2004. С.249

ENHANCED GENERATION OF THZ RADIATION VIA OPTICAL RECTIFICATION OF FEMTOSECOND LASER PULSES ON THE SURFACE OF A NANOCOMPOSITE MEDIUM

M.I. Bakunov, R.V. Mikhaylovskiy

Nizhny Novgorod State University

Optical rectification of ultrashort laser pulses in electro-optic crystals is a proven way to generate broadband terahertz radiation. In this technique, the pump optical pulse produces a nonlinear polarization that follows the envelope of the optical intensity. The nonlinear polarization emits terahertz radiation. Two schemes of the emission are used in experiments – terahertz generation in the bulk of an electro-optic crystal and on the surface of a semiconductor [1] essential drawback of the both schemes is low efficiency of the optical-to-terahertz conversion that does not exceed typically 10^{-6}–10^{-5} [2].

To magnify the nonlinear response, we propose to embed metallic (for example, Ag) nanoparticles into an electro-optic matrix (for example, GaAs). As one can expect, the plasmonic enhancement of the optical field in the vicinity of the nanoparticles can increase significantly the nonlinear response of the matrix.

We consider a generic composite medium containing metallic nanospheres characterized by the dielectric function in the optical range $\varepsilon_{\mathrm{m}}(\omega)$ embedded in an electro-optic matrix with the optical dielectric function $\varepsilon_{\mathrm{h}}(\omega)$ and second-order nonlinear susceptibility $\chi^{(2)}(\omega)$. The size of a nanosphere (~10 nm) is assumed to be much smaller than the optical wavelength, thus, the optical field inside the nanosphere can be treated as homogeneous (the quasistatic approximation). We assume also that the distance between the nanospheres exceeds significantly their size.

The linear effective dielectric function of the composite can be written using the Maxwell-Garnett formula:

$$\varepsilon_{\mathrm{eff}}(\omega)=\varepsilon_{\mathrm{h}}\left[1+\rho\frac{3(\varepsilon_{\mathrm{m}}-\varepsilon_{\mathrm{h}})}{\varepsilon_{\mathrm{m}}(1-\rho)+\varepsilon_h(2+\rho)}\right], \qquad (1)$$

where ρ is the fill-factor associated with a relative volume of nanoparticles. To calculate the effective nonlinear susceptibility of the composite, we write the nonlinear polarization P^{NL} via the local electric field E_{loc} in the matrix: $P^{NL} = \chi^{(2)} E_{loc} E^*_{loc}$, relate the local field to the average field E by means of the equation $E_{loc} = E + 4\pi P/3$, and substitute into the latter formula the linear polarization P as $P = \varepsilon_{eff} E$. Thus, we arrive at the relation $P^{NL} = \chi_{eff}^{(2)} E E^*$ with the effective nonlinear susceptibility given by

$$\chi_{eff}^{(2)}(\omega) = \chi^{(2)} \left| \frac{\varepsilon + 2}{(1-\rho)\varepsilon + (2+\rho)} \right|^2 , \qquad (2)$$

where $\varepsilon = \varepsilon_m / \varepsilon_h$. According to Eq. (2), the resonant enhancement of the effective nonlinear susceptibility can be achieved at

$$(1 - \rho)\varepsilon + (2 + \rho) \approx 0. \qquad (3)$$

Essentially, the resonant increase in the real and imaginary parts of $\varepsilon_{eff}(\omega)$ occurs at the same condition, see Eq. (1). This prevents using the scheme with bulk optical rectification because of a significant distortion of the pump laser pulse. Thus, we are orienting to the optical-to-terahertz conversion on the surface of the composite. We found that Eq. (2) can be conveniently fulfilled for Ti:sapphire laser (~800 nm wavelength) in the composite containing Ag nanospheres embedded in GaAs. Taking $\varepsilon_h = 12.9$ for GaAs and $\varepsilon_m = 6 - \omega_p^2/(\omega^2 - i\nu\omega)$, with $\omega_p = 1.37\times10^{16}$ s^{-1} the plasma frequency and $\nu = 4\times10^{12}$ s^{-1} the damping rate, for Ag we evaluated from Eq. (2) the fill-factor: $\rho \approx 0.025$.

Let us consider now the incidence of a tightly focused (to a size much smaller than the terahertz wavelength) Ti:sapphire laser pulse on the surface of the GaAs/Ag-composite. We calculate the transmitted to the composite optical pulse using the Fresnel formulas in the frequency domain and find the nonlinear polarization induced by the pulse in a thin (~1 μm thick) boundary layer of the composite using Eq. (2). Then, we solve the problem of terahertz emission from a point dipole placed under the surface of the composite and oriented under an angle α with respect to the surface.

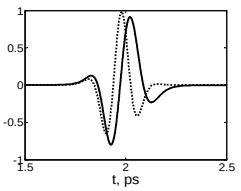

Fig.1

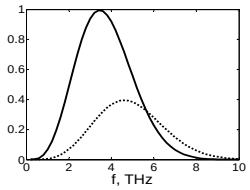

Fig.2

Figures 1,2 show the terahertz waveforms (Fig.1) and terahertz energy spectra (Fig.2) corresponding to the emission from the surface of the GaAs/Ag-composite (solid) and from the surface of unstructured GaAs (dashed) in the normal to the surface direction

for $\alpha = 0$. One can conclude from the figures that inclusion of nanoparticles increases, indeed, the terahertz yield but does not affect significantly the emitted terahertz waveform. The maximum of the energy spectrum for the GaAs/Ag-composite is at ~3.5 THz, while for GaAs it is at 5 THz. Correspondingly, the terahertz pulse duration is slightly larger for the GaAs/Ag-composite than for GaAs. It can be explained by the resonant ringing of the silver nanoparticles after finishing the laser pulse.

[1] Sakai K. (Ed.), Terahertz Optoelectronics, Berlin: Springer, 2005.
[2] Bakunov M.I., Bodrov S.B, Maslov A.V., and Hangyo M. // Phys. Rev. B. 2007, V. 76, P. 085346.

FORMING ANTENNA SYSTEMS OF COMPENSATING CHANNELS ON THE BASIS OF AN ANTENNA ARRAY IN RADAR

I.V. Dushko

Nizhny Novgorod State University

In most up-to-date radar systems for jamming protection an automatic canceller is usually used [1], composed of the main and some auxiliary (compensating) spatial receiving channels that should fulfill following requirements [1]: (1) compensating antennas should have weak directivity (in comparison with the main antenna); (2) the number of compensating channels must be not less than the maximum estimated number of jamming; (3) antenna patterns of compensating channels should have different amplitude and/or phase structure.

When separate antennas are used in the main and auxiliary channels, it makes possible to carry out an effective automatic external jamming canceller. However, in practice, due to the tendency to minimize the device dimensions, the most actual is the case when the compensating channel antennas are based on the antenna array elements (subarrays) of the main channel. Therefore, the list of the requirements should be rather extended.

In this paper, as an example, a linear equidistant antenna array composed of eight elements is examined. The signal of the main channel λ is formed by summing up output signals of all antenna array elements. The compensating channel output signals are formed by partial summing up outputs of elements of the same antenna array. Antenna patterns of the main channel $\lambda(U)$ and compensating channels $x_1(U)$, $x_2(U)$, $x_3(U)$ (Fig. 1) fulfill foregoing requirements under the condition that the maximum number of jamming is equal to three.

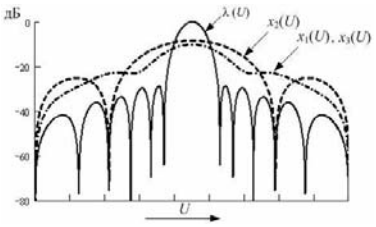

Fig. 1

The procedure of jamming cancellation consists of subtracting a linear combination of jamming in compensating channels from jamming in the main channel. A weight vector **V** of auxiliary channels minimizing the value of jamming output mean power is a

normal (i.e., with minimum norm) solution of the matrix Wiener-Hopf equation [2] and is equal to

$$\mathbf{V} = \mathbf{R}^{+}_{\mathbf{XX}}\,\mathbf{R}_{\mathbf{X}\lambda}, \qquad (1)$$

where $\mathbf{R}^{+}_{\mathbf{XX}}$ is Moore and Penrose pseudoinverse matrix with respect to the correlation matrix $\mathbf{R}_{\mathbf{XX}} = \langle \mathbf{X}\mathbf{X}^{H} \rangle$ of jamming $\mathbf{X}$ in compensating channels; $\mathbf{R}_{\mathbf{X}\lambda} = \langle \mathbf{X}\lambda^{H} \rangle$ is the vector of jamming cross-correlation in the main and auxiliary channels.

Let us examine the case, when the system described above is influenced by three statistically independent external jamming. As far as the jamming number in this case not exceeds the number of compensating channels, at antenna system adaptation all jamming is expected to be efficiently suppressed. However, the computer simulation shows than not only jamming, but also all other signals will be suppressed independently on their directions; i.e., in this case the adaptive (resulting) antenna array pattern $\xi(U)$ is identically equal to zero. Then it is clear that any spatial processing becomes pointless. Besides, the weight vector $\mathbf{V}$ is turned out to be equal to $\mathbf{V}_0 = (1, 1, 1)^{H}$.

In case of one or two external jamming the presence of array blindnesses in the directions U_1 and U_2 of jamming effect signifies that the jamming is suppressed and the negative effect of nulling the whole adaptive antenna pattern does not appear (see Fig. 2), that makes possible to combine jamming nulling with useful (wanted) signal accumulation.

The computer simulation results given in this paper can be explained as follows. As is generally known (e.g., see [2]), the system of Wiener-Hopf equations is always simultaneous, because its right side $\mathbf{R}_{\mathbf{X}\lambda}$ belongs to the image of the matrix $\mathbf{R}_{\mathbf{XX}}$. With three or more jamming the matrix $\mathbf{R}_{\mathbf{XX}}$ is non degenerate and the system of Wiener-Hopf equations has the unique solution which appropriately coincides with the vector $\mathbf{V}_0$ resulting in nulling all adaptive antenna pattern.

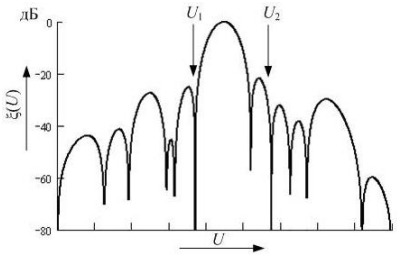

Fig. 2

In case of one or two jamming the rank of matrix $\mathbf{R}_{\mathbf{XX}}$ is incomplete and the infinite set of vectors satisfies the system, in particular there is the vector $\mathbf{V}_0$ among them. However, the solution with the least norm allows to minimize self-noise power added from compensating channels to the main one during jamming suppression. It is easy to show that this solution is the only possible and when there is one or two jamming it does not coincide with the vector $\mathbf{V}_0$, because in both cases it has non-zero projection on the subspace nullified by matrix $\mathbf{R}_{\mathbf{XX}}$. Therefore, nulling an adaptive antenna pattern does not take place.

Thus, to design an automatic canceller of active jamming antenna systems must be formed so, that the main channel antenna pattern would be non-representable in the form of a weighted sum of compensating channel antennas' patterns. Otherwise with the external jamming number equal to or more than the number of compensating channels the adaptive antenna system will suppress all received signals independently on their directions, hence the radar becomes absolutely ineffective.

[1] Ширман Я.Д., Манжос В.Н. Теория и техника обработки радиолокационной информации на фоне помех. М.: Радио и связь, 1981. 416 с.
[2] Балакришнан А. Теория фильтрации Калмана. М.: Мир, 1988. 168 с.

SHORT SIGNALS SPECTRALS ESTIMATION METHOD

E.P. Fradkina

Nizhny Novgorod State University

In this work it is suggested to approximate a discrete signal S_i by a linear combination of P sinusoids of different frequencies, amplitudes, and phases,

$$\widetilde{S}_i = \sum_{k=1}^{P} A_k \cos(\omega_k i + \varphi_k),$$

so as the mean-square error between the model and the signal

$$\varepsilon = \frac{1}{N}\sum_{i=1}^{N}\left|S_i - \widetilde{S}_i\right|^2$$

be at its minimum value.

To solve the problem a virtual instrument was created in LabVIEW programming environment. It uses Nelder-Mead optimization algorithm for optimal parameters of the function search [1]. To shorten the optimal solution search time such parameters as amplitudes and phases are calculated analytically using these expressions

$$\varphi_k = Arctg\frac{Y_k}{X_k}, \qquad A_k = \sqrt{X_k^2 + Y_k^2},$$

where X_k and Y_k can be obtained analytically via the linear equation system solution.

$$\begin{cases} \sum_{k=1}^{P} X_k \sum_{i=0}^{N-1} \cos\omega_k i \cdot \cos\omega_m i - \sum_{k=1}^{P} Y_k \sum_{i=0}^{N-1} \sin\omega_k i \cdot \cos\omega_m i = \sum_{i=0}^{N-1} S_i \cos\omega_m i \\ \sum_{k=1}^{P} X_k \sum_{i=0}^{N-1} \cos\omega_k i \cdot \sin\omega_m i - \sum_{k=1}^{P} Y_k \sum_{i=0}^{N-1} \sin\omega_k i \cdot \sin\omega_m i = \sum_{i=0}^{N-1} S_i \sin\omega_m i \end{cases},$$

m =1, 2, …, P.

Described method is used for time-frequency distribution calculation via the sliding window.

As an example let's consider an experimental signal analysis. The signal was obtained by the set, which consists of a pendulum with a metallic well sound reflective plate, the speakers, a microphone and a computer [2]. The microphone and the speakers are connected to suitable computer inputs. The microphone is situated between the radiating sinusoidal signal speakers and a pendulum so as the sound radiated by the speakers be

reflected from a swinging plate and hit upon it. The signal from the microphone is recorded on a computer disk as a file.

The obtained signal is interesting for us due to the fact that besides a reference frequency component of the signal radiated by the speakers there is a weaker frequency component of Doppler-shifted sound signal reflected from a swinging plate. Doppler frequency shift is not more than 15 Hz at the reference signal frequency of 4410 Hz and the maximum plate speed of 0.5 m/sec.

To reduce the influence of interfering sound signals and to shorten the calculation time the obtained signal was preprocessed by a band-pass filter, a synchronous detector, and then decimated. For time-frequency the distribution calculation the sliding window of 150 samples was used.

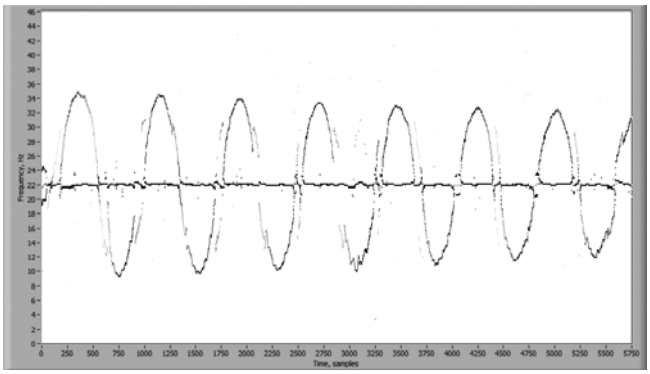

Fig.

The distribution is shown in the figure. The time is taken to the abscissa axis in samples; the frequency is taken to the axis of ordinates which corresponds to the rate of the movement of a plate from -0.5 m/sec to +0.5 m/sec.

Two frequency components are well seen in the distribution, one of them corresponds to the frequency of the signal from the speakers, the other corresponds to the frequency of the signal reflected from a moving plate.

The method is good for short discrete signals analysis and can be used for time-frequency analysis. High resolution can be achieved both over the time and frequency range. The disadvantage is that the method requires much time for calculation.

[1] Лупов С.Ю., Фрадкина Е.П. /Труды международной научно-практической конференции ″Образовательные, научные и инженерные приложения в среде LabVIEW и технологии National Instruments” М.: Изд-во РУДН, 2006. С. 278.

[2] Lupov S.Yu., Fradkina E.P. //Труды XI научной конференции по радиофизике/ Под ред. А.В.Кудрина, А.В.Якимова. Н. Новгород: Изд-во ННГУ, 2007. С. 270.

EXPERIMENTAL ANALYSIS OF COLLISIONS IN WIRELESS SENSOR NETWORK

A.A. Kiryushin, A.N. Sadkov

Nizhny Novgorod State University

This paper provides a deeper understanding of concurrent transmissions and Clear Channel Assessment in CSMACA-based WSN.

Conventional knowledge is that in CSMACA-based WSN collisions happen because of a hidden terminal [1]. However, the situation when nodes start transmitting at the same time may also lead to collision. The definition of ”at the same time” depends on details of the CCA implementation in the particular transmitter. In the 802.15.4-compliant CC2420 transceiver [2] - used by many WSN platforms – current CCA result is calculated on the basis of channel measurement over the last 0.128ms. The CCA mechanism may fail to detect busy channel if transmissions started less than 0.128ms before CCA sampling.

In our experiments we used TmoteSky motes equipped with 802.15.4-compliant CC2420 radios operating at 2.4GHz. Fig. 1 shows our experimental configuration. Each experiment involves two senders, one receiver and one synchronizer mote. The nodes were placed so that transmitters could hear each other, i.e., there were no hidden terminals. Experiments were carried out in a closed room with no movement. The nodes operated on channel 26, and no active 802.11 devices were present. Two types of experiments were carried out without channel access algorithm, and employing CSMACA algorithm. In the first case CCA was intentionally disabled (and hence CSMACA) on transmitting nodes.

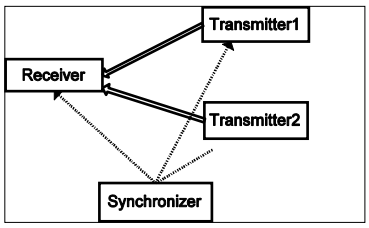

Fig. 1

The synchronizer sent a synchronization packet before series of concurrent packet transmissions. This served to synchronize the clock of motes. After reception of the synchronization packet each transmitter launched the timer. Every time the timer fired, the node attempted to transmit a packet. In experiments without CSMACA, the node sent a packet immediately; otherwise it performed CCA first and deferred transmission if the channel was busy. The timer consecutively started 7000 times on each transmitter. The time interval between timer firings was 4ms plus random value from interval 0 to 3ms. In that case of disabled CSMACA the beginning of packets transmissions always coincided with timer firings (this is not true when CSMACA is enabled). If CSMACA is enabled and the timer fired when the previous packet was not sent because of a busy channel, then a new packet was rejected. Each transmitter kept track of quantity of rejected packets.

The CC2420 has a built-in Clear Channel Assessment pin which is used to implement the CSMACA functionality. This pin is sampled by communication software to detect if other nodes are sending. The energy detector computes the average power of a signal over the last 0.128ms.

Assume that the node is attempting to send a packet less than 0.128ms after the other node started transmission (see Fig. 2). The current CCA pin value is a result of channel measurement over the last 0.128ms. During this time interval the node at first was receiving noise (interval AB), then it was receiving another node signal (interval BC). Averaged over 0.128ms power will be smaller than the power of the signal since the signal was summed with noise, moreover, the average power may be smaller than the CCA threshold, i.e., CCA may not detect presence of transmission.

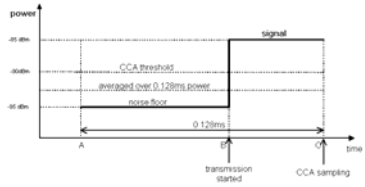

Fig. 2

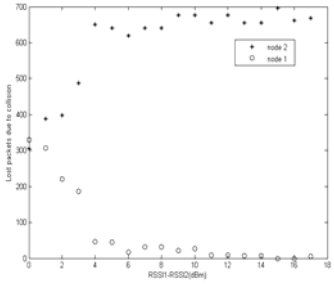

Fig. 3

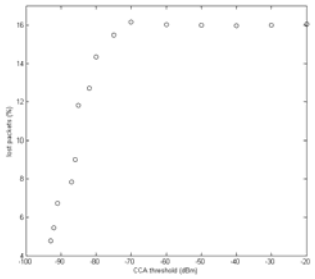

Fig. 4

Our experiments with motes with CC2420 radios show (Fig. 3) that collisions often occur even when two concurrent transmitters can hear each other. In very simple traffic models from 2% to 16% of transmitted packets, depending on the CCA threshold, were lost due to collisions. Our results also indicate that at such collision only the packets from the node with the weaker signal are lost because of capture effects, in contrast to a collision that happens due to hidden terminal, when both packets can be lost. It was found (Fig. 4) that near the noise floor CCA threshold allows us to reduce the number of such collisions and showed that simple model is sufficient to take these effects into account in simulation. These findings should be considered while developing MAC protocols and channel models, especially for those expected to operate under high traffic.

[1] Ye W., Heidemann J. Medium Access Control in Wireless Sensor Networks/ Ed. C. S. Raghavendra, K. Sivalingam, T. Znati. Kluwer Academic Publishers, 2004. Chapt. 4. P. 73.
[2] CC2420 Datasheet (rev. 1.3)

AN ALGEBRAIC APPROACH TO QUANTUM LIOUVILLE EQUATIONS

D. N. Kobyakov

Nizhny Novdorod State University

The purpose of this article is to introduce a computational method which can be helpful while describing an interaction of a quantum system with fluctuating electromagnetic field. The developed method is constructed naturally within an algebraic approach to quantum Liouville equations. The first result of using the method is the exact solution of quantum Liouville equation for a two-level system that is described by a time-independent Hamiltonian; for the author's knowledge this solution was not previously reported. Furthermore the method was successively used for computations within the problem of relaxation of a two-level system, elucidated by Fox and Faid [1].

Relaxation essentially is *irreversible* approaching of the system to thermodynamical equilibrium. Reversible Liouville equations with stochastic coefficients reveal irreversible dynamics only after averaging.

Within the algebraic approach to Liouville equation the operation of commutation of Hamiltonian and density matrix will be treated as an operator (commutator) acting upon density matrix (as well as abstract algebraic operators will be introduced, see below). Due to linearity of commutation this can be depicted as follows:

$$i\hbar\frac{\partial}{\partial t}\hat{\rho}_{\alpha\beta}(t)=\sum_{\alpha'\beta'}[\hat{H}_0+\hat{\tilde{H}}(t),\cdot]_{\alpha\beta\alpha'\beta'}\hat{\rho}_{\alpha'\beta'}(t)\,. \qquad (1)$$

Hamiltonian as well as density matrix of a two-level system are expanded in terms of Pauli matrices. The set of Pauli matrices is a basis since it is a linear combination of the *natural basis* of the class of 2×2 matrices, namely:

$$\sigma_{11}=\begin{pmatrix}1&0\\0&0\end{pmatrix},\ \sigma_{12}=\begin{pmatrix}0&1\\0&0\end{pmatrix},\ \sigma_{21}=\begin{pmatrix}0&0\\1&0\end{pmatrix},\ \sigma_{22}=\begin{pmatrix}0&0\\0&1\end{pmatrix}\qquad\text{and}$$

$$\sigma_0=\sigma_{11}+\sigma_{22}\,,\quad \sigma_1=\sigma_{12}+\sigma_{21}\,,\quad \sigma_2=i\sigma_{21}-i\sigma_{12}\,,\quad \sigma_3=\sigma_{11}-\sigma_{22}\,.$$

Within a class of $N\times N$ matrices one can define *basis* σ_{ij} in a similar way:

$$\{\sigma_{ij}\}_{\alpha\beta}=\delta_{i\alpha}\delta_{j\beta}\,. \qquad (2)$$

Here $\{\ \}_{\alpha\beta}$ denotes the $\alpha\beta$-matrix element and $\alpha,\beta,i,j=1,2,...,n$. After that define *basis operators* $D_{ij;kl}$, for the space of commutator operators, by their action upon the basis (that is the set σ_{ij}) of the operand of commutation (expanded density matrix):

$$D_{ij;kl}\sigma_{mn}=\delta_{km}\delta_{ln}\sigma_{ij}, \qquad (3)$$

where $i,j,k,l,m,n=1,2,...,N$.

The set $D_{ij;kl}$ is the basis since commutation is a linear operation. With this definition it is easy to show that

$$D_{ij;kl}D_{mn;pq}=\delta_{km}\delta_{ln}D_{ij;pq}\,. \qquad (4)$$

Now one can see that if a commutator is written as an expansion in terms of the set $D_{ij;kl}$ with appropriate coefficients and if then this expansion *is depicted* as a $N^2 \times N^2$ matrix, then, due to the latter formula, a multiplication with another commutator can be handled using *common matrix-multiplication rules*.

Now the exact solution for Quantum Liouville Equation for a two-level system that is described by a time-independent Hamiltonian will be shown. The Liouville equation is: $i\hbar \frac{\partial}{\partial t}\hat{\rho}(t) = [\hat{H}_0, \hat{\rho}(t)]$, where $\hat{H}_0 = i\hbar(a\hat{\sigma}_0 + b\hat{\sigma}_1 + c\hat{\sigma}_2 + d\hat{\sigma}_3)$ and a,b,c,d are constant complex values. The equation transforms into $\frac{\partial}{\partial t}\hat{\rho}(t) = (bT_1 + cT_2 + dT_3)\hat{\rho}(t)$ if one depicts $T_i = [\sigma_i, \cdot]$. The solution can be easily written:

$$\hat{\rho}(t) = \exp[bT_1 t + cT_2 t + dT_3 t]\hat{\rho}(0) . \qquad (5)$$

Now it is clear that since the initial conditions can be given as unique expansion in terms of Pauli matrices with some constant coefficients, then to get the final solution for $\hat{\rho}(t)$ we need to know the action of that exp[…] uniquely upon each of Pauli matrices. This action one gets with the help of the method:

$$e^{\alpha T_1 + \beta T_2 + \gamma T_3} \cdot \sigma_0 = \sigma_0 ,$$

$$e^{\alpha T_1 + \beta T_2 + \gamma T_3} \cdot \sigma_1 = \{+1 + BR_{23}{}^2\}\sigma_1 + \{+i\gamma A - \alpha\beta B\}\sigma_2 + \{-i\beta A - \alpha\gamma B\}\sigma_3 ,$$

$$e^{\alpha T_1 + \beta T_2 + \gamma T_3} \cdot \sigma_2 = \{-i\gamma A - \alpha\beta B\}\sigma_1 + \{+1 + BR_{13}{}^2\}\sigma_2 + \{+i\alpha A - \beta\gamma B\}\sigma_3 , \qquad (6)$$

$$e^{\alpha T_1 + \beta T_2 + \gamma T_3} \cdot \sigma_3 = \{+i\beta A - \alpha\gamma B\}\sigma_1 + \{-i\alpha A - \beta\gamma B\}\sigma_2 + \{+1 + BR_{12}{}^2\}\sigma_3 ,$$

where $A = \frac{1}{R_0}\mathrm{sh}(2R_0)$, $B = \frac{1}{R_0{}^2}[\mathrm{ch}(2R_0) - 1]$, $R_0 = \sqrt{\alpha^2 + \beta^2 + \gamma^2}$,

$$R_{12}{}^2 = \alpha^2 + \beta^2 , R_{13}{}^2 = \alpha^2 + \gamma^2 , R_{23}{}^2 = \beta^2 + \gamma^2 . \qquad (7)$$

It would be useful to consider a special case when $\alpha = \beta = 0$. One can get easily with *explicit* computation that (for n=0, 1,2,...) $T_3{}^{2n+2} = 4^n T_3{}^2$ and $T_3{}^{2n+1} = 4^n T_3$. After that an exercise of a little algebra yields $e^{\gamma T_3} = 1 + \frac{1}{2}\mathrm{sh}(2\gamma)\cdot T_3 + \frac{1}{4}[\mathrm{ch}(2\gamma) - 1]\cdot T_3{}^2$, which in fact is in accordance with the general expansion (6) with $\alpha = \beta = 0$. Due to the fact that the last formulas have been derived explicitly, by the investigation of their action upon Pauli matrices, one may conclude that the new method provides correct solution.

[1] Faid K., Fox R.F. // Phys. Rev. A. 1986. V. 34. P. 4286.

CLUSTER ANALYSIS OF ASTROCYTE ACTIVITY

A.S.Pimashkin, A.V.Semyanov, A.A.Lebedinsky

Nizhny Novgorod State University, RIKEN Brain Science Institute

For many years glial cells were considered to be supporting glue for the neuronal networks and their functions were limited to nutrition, protection and homeostasis maintenance of neighboring neuronal networks. It was discovered that neuronal and astrocytic networks can communicate to each other via diffuse signals. To find out how astrocytes may influence neuronal signal propagation, first we need to establish principles of activity pattern formation in the astrocytic networks. Here we present an approach which allows numerical analysis of experimental data obtained with laser scanning confocal calcium imaging. The approach allows detection of calcium oscillations in a stack of sequential images and finding correlations between signals in neighboring cells.

To study astrocytic activity we used hippocampal slices obtained from rats and mice.

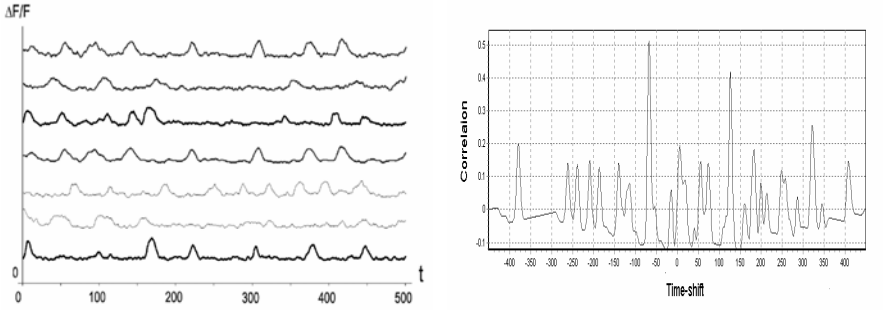

Figure 1. (Left) Calcium oscillations detected from active astrocytes processed with a low-pass filter and biased appropriately. (Right) Cross-correlation function of activities of two cells

Figure 1 shows calcium oscillations recorded from several active astrocytes separated from neurons. To search for specific patterns of the astrocytic calcium activity and astrocyte-to-astrocyte signal propagation we applied cross-correlation analysis and shuffle-test. At first, varying time shift, we find a maximum of correlation between two signals.

$$K(x,y) = \frac{\sum_{i=1}^{T}(x_i - \langle x \rangle)(y_i - \langle y \rangle)}{(T-1)\delta_x^2 \delta_y^2}$$

where x , y – fluorescence in the first and the second astrocyte, T – recording time (~7 minutes). Because certain delay is introduced by signal propagation from an astrocyte to another astrocyte we applied time-shift correlation function, $K(x(t),y(t+\tau))$.

Next we change the sequence of pulses in time by randomizing delays between pulses and find a new maximum of correlation. Such procedure repeats about 1000 times. After that we can plot distribution of correlation maximums (fig 2).

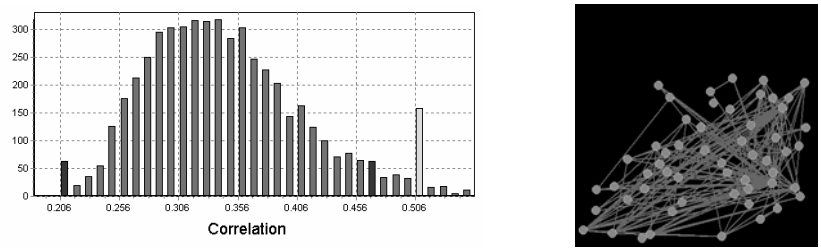

a b

Figure 2. (a) Distribution of correlation maximums in shuffle-test. (b) Reconstructed architecture or spatial-temporal pattern of astrocytic activity

Resulting distributions remind of Gaussian form, where we can find median standard deviation. Then if a maximum of correlation between original activities is more than the standard deviation, we can say that the pair of cells is connected and a part of an activity pattern transmits from one cell to another during specific time delay. Using this method for determining connections between cells we can rebuild an architecture or a pattern of the astrocyte activity (Fig. 2(b)). For instance, if two astrocytes express the maximal correlation without any time shift they may be driven from the same source outside of the focal plane. In addition to the time shift of the maximal correlation we can directly measure the distance between pairs of astrocytes.

To understand the mechanisms of forming astrocyte networks and to prove that such networks are not random we used clustering analysis. The cluster coefficient characterizes the fraction of friendship connectivity or connectivity of neighbours. For example complete graph has the clustering coefficient 1 and random networks 0. But small-world networks have attributes of both of them and have the clustering coefficient ~0.5.

To analyze the network configuration changes we made the following experiment. Pharmocological drug Tetrodotoxin (TTX) is known to be a blockator of action potential propagation in neuronal netwoks. We calculated the cluster coefficient before and after applying TTX to astrocytes. After TTX the clusterisation of the network reduces and the number of significantly correlated pairs of cells is also reduced. In the same conditions (the average number of pulses in the slice, the number of pulses per cell, etc) the configuration and clusterisation of an astrocytic network changes due to the blocking one of the types of connections in an astrocytic network - information propagation via neuronal networks. These principles will be included in the two-layer model of a neuron-glia network.

Acknowledgements
Supported by Russian Foundation for Basic Research (grant 08-02-00724, 08-04-97109).

SPIKE-TIMING PATTERNS IN NETWORKS OF SYNAPTICALLY COUPLED NEURONS WITH AXONAL CONDUCTION DELAYS

A.Yu. Simonov

Nizhny Novdorod State University

Investigating principles of information processing in biological systems still remain one of the most interesting branches of modern science. It is widely believed that in the brain, information is represented in form of various spatio-temporal patterns of neuronal activity. In this study, mechanism of pattern generation using geometry of the network with axonal conduction delays has been proposed.

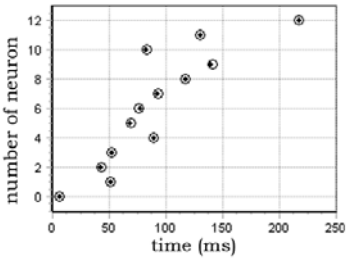

Fig. 5

Hodgkin-Huxley [1] neurons were chosen as units of the network. Each neuron is in excitable mode and its membrane potential remains constant without external stimulations. Signal propagation delay is proportional to physical distance between two cells.

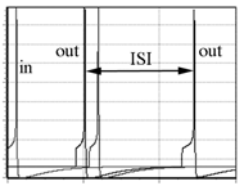

Fig. 2

The following example illustrates how to generate the simplest pattern consisting of two spikes with certain interspike interval (ISI). The fragment of the network architecture is depicted in fig.1. Single input pulse produced can propagate through the network, transforming and evoking various patterns of neuron activity. Fig.2 illustrates evolutions of membrane potentials of three neurons represented in fig.1. If random sequence of input pulses with uniformly distributed ISI has been given the output distribution of ISI is as in fig.3. Here one can see the distribution with pronounced peak. Thus, the network fragment presented can select certain ISI from uniformly distributed ISI probability.

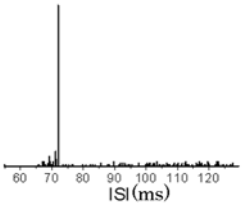

Fig. 3

In modeling networks consisting of hundred of neurons stable spatio-temporal patterns can be found. Geometry of the network (axonal conduction delays) and the dynamical properties of local cells (e.g. refractory period) underlie the appearance of those patterns.

To find the patterns various inputs should be considered and all the possible paths of signal propagation should be traced. Each path evokes pattern occurrence and hence activation of neuron group that corresponds to appropriate input stimulus. It is noteworthy that the number of such groups can be far greater than the number of the neurons. That is why there is an unprecedented memory capacity in the brain.

Fig.4 represents the architecture of the network used for testing patterns finding algorithm. The input neuron pointed the arrow receiving a single stimulus generates an action potential that propagates to the next three neurons and excites them. The next neurons transfer an excitation only if they receive it simultaneously. It requires matching axonal conduction delays. Thus, the signal propagates from one neuron to another and decays when there is no next neuron with converging delays. The tested network depicted in fig.4 has been constructed so that it contains only one polychronous group consisting of all the neurons of the network. A polychronous group is characterized with the order of its neuron firing and the time of each neuron firing (spike-timing). The found group of the tested network is represented in fig.5 with the help of a raster. Here the circles represent spike timings of neurons comprising the polychronous group and the small dots represent the spike-timing pattern that occurs during simulation after input stimulus. As one can see, there is coincidence between the found pattern and the generated one.

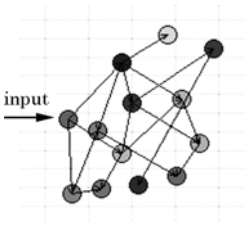

Fig. 4

Another example illustrates the raster of one of numerous polychronous groups that exist in the network of 150 neurons (fig.6). In such networks, certain input stimulus activates one or several groups and a certain spike-timing pattern emerges. In other words, the network is capable of storing information in the form of polychronous groups and retrieving it when the group activates. Information is memorized due to synaptic plasticity mechanism that is not taken into account in this study.

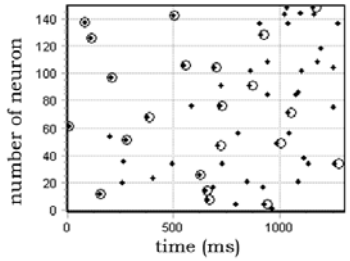

Fig. 6

Adding certain biologically relevant features such as synaptic plasticity and influence of glia should enrich dynamics of such networks. Having solved the problem of encoding input/output information, we will approach making model for some cognitive functions.

This work was supported by Russian Foundation for Basic Research (grant 08-02-00724, 08-04-97109).

[1] Hodgkin A.L., Huxley A.F. //J. Physiol. 1952. V.117. P. 500.